JMEPEG (2012) 21:1526–1533
DOI: 10.1007/s11665-011-0050-x

1059-9495/$19.00

Microscopic Mechanism of Strengthening Under Low-Amplitude Loads Below the Fatigue Limit

Songlin Zheng and Xi Lu

(Submitted January 13, 2011; in revised form May 18, 2011)

Using scanning electron microscopy, transmission electron microscopy, and X-ray diffraction, some microscopic experiments and analyses were performed to explain the microscopic mechanism of strengthening under low-amplitude loads below the fatigue limit (SLAL). The experimental results show that the microscopic mechanism of SLAL could be dislocation-accumulation and grain boundary strengthening to low-strength material without strengthening by surface heat treatment. After SLAL, the microstructure imperfections can be improved and the fatigue resistance can be enhanced. Macroscopically, the fatigue strength and life of structures can be obviously improved and increased.

Keywords fatigue life, fatigue strength, fractography, low-amplitude loads below the fatigue limit, microscopic mechanism, strengthening

1. Introduction

It has long been known that the fatigue limit for some metals may be improved by understressing, followed by a process of gradually increasing the amplitude of the applied alternating stress in small increments, this procedure is normally called coaxing, and it is also named understressing (Ref 1). The phenomenon of strengthening under low-amplitude loads below the fatigue limit (SLAL) is that the fatigue strength, also including static strength and yield strength, and fatigue life of metallic materials and structures exhibiting the coaxing effects can be increased by applying proper low-amplitude loads below the fatigue limit and proper strengthening cycles.

The strengthening phenomenon of low-amplitude loads below the fatigue limit was first investigated using standard specimens in the USA and England during the last century (Ref 1, 2). Sinclair (Ref 2) discovered that not all metallic materials could exhibit such a large increase in fatigue strength and fatigue life due to the coaxing effect. Only materials capable of strain aging could be strengthened in such a manner. Using standard material specimens, the fatigue limit of low carbon steels can be increased nearly 30% (Ref 1), and the fatigue life to 14 times that of 40MnB steel tempered at 200 °C (Ref 3). However, the process of understressing was also considered impractical for coming generations (Ref 4). Hence, in-depth investigations of this phenomenon were not popular.

After World War II, using standard material specimens, many Japanese researchers began to investigate the strengthening effects of different metallic materials and heat treatment processing through the JSMS Committee on Fatigue of Materials (Ref 5–12). It was found that the mechanism of the SLAL was possibly micro-plastic deformation or work hardening (Ref 5–7). Some experiential equations had also been established, with which the strengthening effects of low-amplitude loads below the fatigue limit could be considered in spectrum loading (Ref 8, 9). However, the microscopic mechanism and the engineering application of SLAL have rarely been investigated.

During fatigue experiments of vehicle components or parts, we have found that not only fatigue strength, but also static strength, yield strength, hardness, natural frequency, and fatigue life can be clearly changed and improved by the SLAL (Ref 10), such as front axles (Ref 11), transmission gears (Ref 12), crankshafts (Ref 13), pedrails (Ref 14), and drive shafts (Ref 19). The amount of increases in the fatigue life and strength is clearly lower in actual vehicle components as compared to that for standard material coupon specimens. The strengthening cycles of actual vehicle structures with remarkable strengthening effect range from 200,000 to 400,000 cycles, which is much less than that of standard material specimens, with about 10,000,000 cycles. There is an obvious region of load and cycles with strengthening effects as well as the optimal strengthened load and cycles for the actual vehicle component. The strengthening effects were also observed in the block spectrum loading with alternating high and low amplitudes and the random spectrum loading (Ref 15). The simple strengthening conditions make possible for us to apply the strengthening effects of the SLAL in engineering.

In actuality, the phenomenon and mechanism behind the SLAL are still under investigation. The materials still include high strength steel (Ref 15–17), aluminum alloy (Ref 18), 70 w/o Cu-30 w/o Zn brass alloy (Ref 19), Zr-based bulk-metallic glass (Ref 20) and so on. Although there are a considerable number of the fatigue experiments on the SLAL, there are few system reports discussing the micro-mechanism of the SLAL. Only non-propagating cracks (Ref 21), micro-structural changes (Ref 22), grain sizes (Ref 23) have been considered and partially investigated.

Songlin Zheng and **Xi Lu**, Institute of Vehicle Engineering, College of Mechanical Engineering, University of Shanghai for Science and Technology, No. 516 Jungong Road, Shanghai 200093, China. Contact e-mail: luxi_usst@163.com.

In this paper, mechanical experiments of fatigue and SLAL were performed using vehicle front axles, a kind of low carbon steel, to exhibit the strengthening effects, while metallographic experiments on some typical specimens by using scanning electron microscopy (SEM), transmission electron microscopy (TEM), and X-ray diffraction (XRD) were performed to investigate the corresponding micro-mechanism of the SLAL.

2. Material and Experimental Procedures

In order to eliminate differences in manufacturing processes, heat treatments, and dimensions as much as possible, actual front axles of a light truck were used to investigate the phenomenon and microscopic mechanism of the SLAL. The front axle, welded with the seamless steel pipe, is a low-strength material without any surface heat treatment. The material of the front axle is 20 steel, with the chemical compositions listed in Table 1. Its elastic modulus is 200 GPa, yield strength is 324 MPa, Poisson's ratio is 0.3, and the yield strength ratio is 0.69.

The primary purpose of this paper is not to perform an accurate quantitative analysis of the microscopic mechanism, but to make a comparative study of the micro-mechanism under different strengthening loads and strengthening cycles. All specimens of micro-experiments are the typical result of strengthening experiments.

Fatigue and strengthening experiments were performed on the same electro-hydraulic servo fatigue testing machine—TT100 fatigue machine. A sinusoidal waveform signal with a frequency of 6 Hz was used for the constant stress amplitude control, and the stress ratio was 0.1. The repeated cycles of the front axle to final fracture was defined as the fatigue life (Ref 11).

The changes and characteristics of the pore, secondary crack, fatigue striation, beach mark, and crack spacing of the different specimens before and after strengthening under low-amplitude loads were observed and compared with a Leica S440i SEM. Dislocation arrangements in different specimens were investigated with a Hitachi H-800 TEM. A D/Max-RB X-ray was used to analyze the diffraction pattern.

The sampling location for the TEM specimen, which is critical at the maximum stress region, was close to the surface layer and was kept as far away from the clamping region as possible. The sampling direction was axial because the axial stress component was predominant.

3. Results and Analysis

3.1 Strengthening Experiments (Ref 11)

The basic data estimating the strengthening effect of the SLAL is the fatigue life from the virgin *S-N* curve of the front axle. The strengthening effects will be exhibited if the fatigue life of the front axle after SLAL is much greater than that of the virgin *S-N* curve.

Table 1 Chemical composition of the front axle, wt.%

C	Si	Mn	Cr	S	P	Ni	Cu
0.17-0.24	0.17-0.37	0.35-0.65	≤0.25	≤0.035	≤0.035	≤0.25	≤0.25

The results of *S-N* curve experiment under fatigue load amplitude of 185 MPa are shown in Table 2. Under this load amplitude, partially experimental results of front axle after strengthening under different strengthening loads and cycles are shown in Table 3.

In Table 3, the fatigue life is obtained under load amplitude of 185 MPa after strengthening under different strengthening loads and cycles. From the strengthening experiments, it can be concluded that the optimal number of strengthening cycles is about 200,000 cycles and the optimal strengthening load amplitude is about 130 MPa. The longest average fatigue life after SLAL is about 630,000 cycles under a load amplitude of 185 MPa. In the virgin *S-N* curve, corresponding to such a fatigue life, the load amplitude is 165 MPa. After SLAL, the increased percentage of fatigue strength P_s and fatigue life P_N is calculated as follows:

$$P_s = \frac{185 - 165}{165} \times 100\% \approx 12\%$$

$$P_N = \frac{630,000 - 310,000}{310,000} \times 100\% \approx 103\%$$

So, using the SLAL, the maximum amount of increase in the bending fatigue strength for the front axle is about 12%, while the maximum increase in the bending fatigue life for the front axle is in excess 100%.

3.2 SEM Experiments

The specimens selected for SEM analyses are listed in Table 4. The objective of SEM analyses is to compare the

Table 2 Results of partial *S-N* experiments

Fatigue load, MPa	Fatigue life, cycles	Average life, cycles
185	369,000 314,000 258,300	310,000

Table 3 Results of partial strengthening experiments

Strengthening load, MPa	Strengthening cycles, cycles	Fatigue life at 185 MPa, cycles	Average life at 185 MPa, cycles
146	300,000	251,600 123,100 358,200 391,400	256,700
130	300,000	498,400 392,100	445,300
130	600,000	318,400 301,600	310,000
130	450,000	215,200 496,000 358,200	356,500
130	200,000	855,500 356,500 668,000	630,000
115	300,000	248,500 331,900	290,200

variation in microstructures among the different specimens with or without SLAL.

The main factors considered as variations in the microstructure include the number and characteristics of pores, secondary cracks, fatigue striations, beach marks, and fatigue regions of the fatigue fracture, which were mainly observed and analyzed by SEM. The strengthening mechanism of the SLAL was then qualitatively or quantitatively inferred from the changes in the above-mentioned characteristics, among the different experimental specimens, with or without SLAL. The typical results obtained by SEM on different specimens after fatigue fracture are listed in Table 5.

As can be seen from Table 5, the amounts of pores and secondary cracks are referred to the maxima detected in the observed region nearby the fatigue source. Obvious differences in the fracture characteristics are exhibited with or without strengthening, such as the obvious decreases in the number of pores, the maximum diameter of pores, and the size of secondary cracks. This happens if the specimen is strengthened at the optimal strengthening load for the optimum number of cycles. The pore features near the crack sources of No. 012 and No. 035 are shown in Fig. 1.

Table 4 Specimens of SEM analyses

No.	Strengthening conditions	Strengthened load, MPa	Fatigue life, cycles
011	No strengthening	0	314,000
012	No strengthening	0	258,300
034	Optimal strengthening	115	331,900
035	Optimal strengthening	130	498,400

Figure 1 shows that if a specimen is strengthened by the optimal strengthening load and the optimum number of cycles, the pores in fatigue fracture surfaces become increasingly smoother, and the defects in the virgin material are clearly decreased after fatigue fracture. There are no obviously connection pores in No. 035 after strengthening with the optimal strengthening effect. At the same time, the number of pores is clearly decreased after SLAL.

The change of the pore characteristics in the fractured cross-sections implies that the microstructure is strengthened and its local micro-defects are reduced. The local micro-density may be increased because the positions of the virgin pores are filled by a circumambience of metal crystals during the SLAL. This mends the pore and strengthens the weak area in the specimen. It shows that the microstructures can be improved when the strengthening loads and strengthening cycles are appropriate. Hence, the fatigue strength and fatigue life of the specimens after SLAL exhibit an increase and improvement in macro properties. However, the entire macro-density of the specimen remains unchanged.

Figure 2 shows the distribution of secondary cracks of No. 012 and No. 035 after SLAL, the more connection cracks and fewer secondary cracks are clearly observed at the fracture cross-sections. Unfortunately, the obvious change of secondary

Table 5 Typical results of fatigue fractured specimens

No.	Fatigue region, mm	Amounts		Characteristics		
		Pore	Secondary crack	Maximum diameter of pores, μm	Secondary crack	Beach mark
011	5.23	17	13	8.5	Large	0.5-1.52 mm, 6 strips
012	6.27	25	17	9.5	Large	0.5-1.42 mm, 7 strips
034	6.04	1	8	7.74	Narrow	0.5-1.34 mm, 7 strips
035	8.79	5	6	4.9	Narrow	0.5-1.0 mm, 11 strips

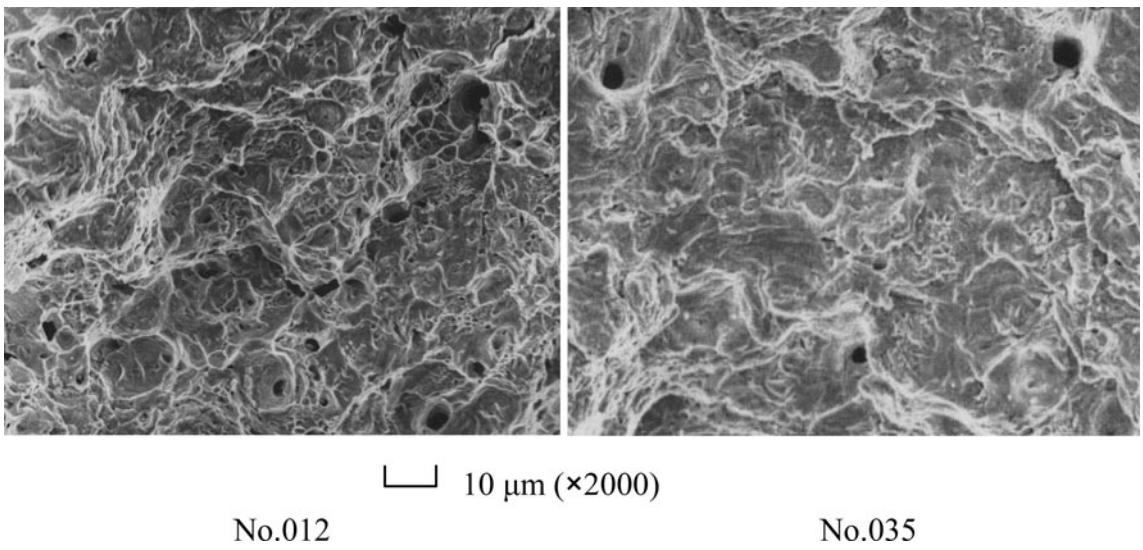

Fig. 1 Pore characteristics of different specimens

cracks is not exhibited in Fig. 2. This can qualitatively be explained as follows. After SLAL, the material becomes increasingly compact and uniform; the integrated force between atoms possibly becomes larger; the structure strength is improved; and the fatigue damage is reduced. When a main crack propagates, its ability to produce secondary cracks in the direction vertical to the main crack is reduced. Hence, the attenuation of fatigue strength is delayed in the most critical cross-section. Thus, the fatigue life of specimens is increased to the same degree if the SLAL is performed in advance.

In Table 5, the initial location of fatigue region was that the distance of beach mark achieved 0.5 mm. The data in Table 5 show quantitatively that the defects in the virgin microstructure such as pore diameters, secondary cracks, and so on are mended and improved by the SLAL. Figure 3 shows the increase in the distance between beach marks for different specimens, where the last value of the distance between beach marks corresponds to the final beach mark of the fractured cross-section.

In fatigue analysis, the rate of fatigue crack propagation can be roughly evaluated by the fatigue striation in the fractured cross-section. At different measured positions for which the radial distance from the fatigue source is 2.5 mm, the average distances between fatigue striations of No. 012 and No. 035 are listed in Table 6.

From Fig. 3 and Table 6, it can be estimated that the rate of crack propagation in No. 035 with the optimal strengthening is lower than that in No. 012 without any strengthening. There are only 6 to 7 strips of beach marks on specimens without SLAL when the front axle is fractured. Hence, the distance between beach marks increased along with fatigue crack propagation. The rate of crack propagation is accelerated during the end of crack propagation. There are 11 strip beach marks on No. 035. There is no obvious change in the distance between beach marks. These results show that fatigue crack initiation is postponed; the rate of crack propagation is decreased, thus enhancing fatigue resistance.

According to the results and analysis of the experimental SEM, the mechanism of the SLAL is as follows: after SLAL, the pores in the virgin material could become smaller. The secondary cracks in the virgin material could become lesser and thinner and the microstructure of the virgin material could become more uniform and compact. The change in the microstructure postpones the fatigue crack initiation and propagation. Hence, the fatigue strength and fatigue life of the front axle are increased and improved by the SLAL.

3.3 TEM Experiments

Specimens for the TEM experiments were made from No. 000, No. 012, and No. 035. Specimen No. 000 is the virgin condition of the front axle. The sampling location of TEM experiments is the region of the maximum tensile stress. The sampling direction is axial because the stress component in axial direction is larger than those in the other directions. The typical results of the dislocation distribution in the different specimens are shown in Fig. 4.

For specimen No. 000, the dislocation structure in the virgin specimen is sparse and discrete, mainly located within the grain interiors and nearby grain boundaries. However, some dislocations within individual grain interiors are also observed in the

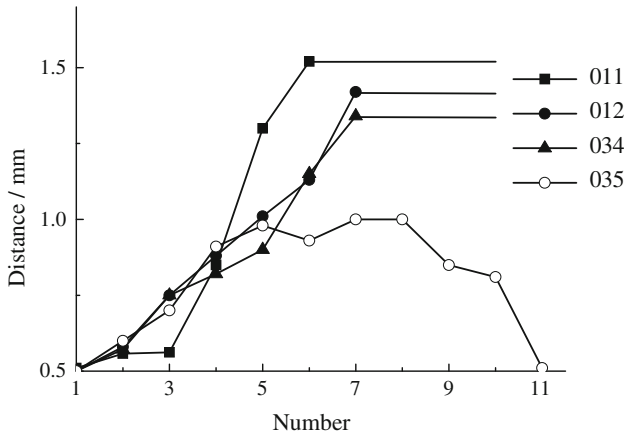

Fig. 3 Variation of beach marks of different specimens

Table 6 Distance between fatigue striations, μm

No.	1	2	3	Average
012	0.349	0.350	0.400	0.366
035	0.302	0.303	0.305	0.303

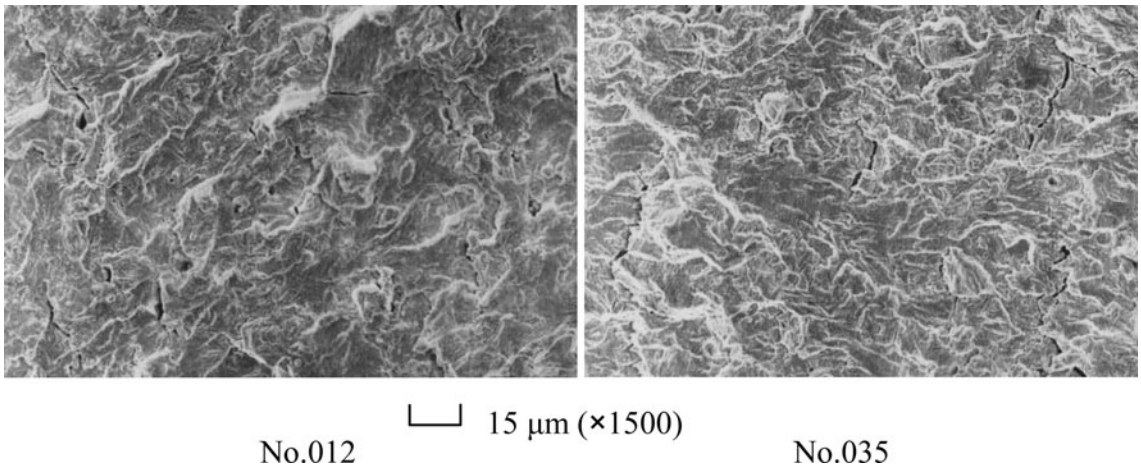

Fig. 2 Secondary cracks of different specimens

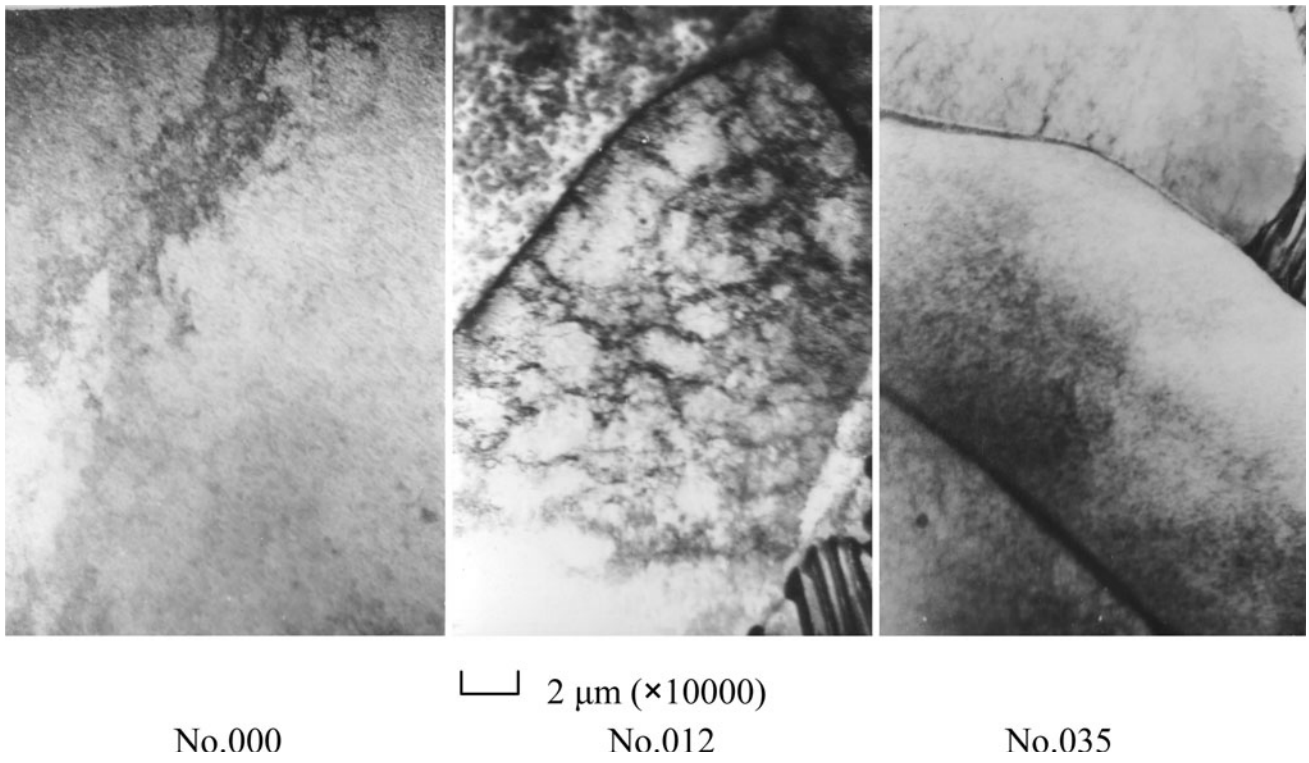

Fig. 4 Dislocation changes in different specimens

virgin material. With specimen No. 012, which is directly fractured at the fatigue load, there are many regular and high-density dislocations in the grain interiors and nearby grain boundaries. A greater number of patch dislocations are observed within grain interiors. In the specimen No. 035, which fractured at load amplitude of 185 MPa after strengthening at the optimal strengthening load for the optimum number of cycles, dislocations mainly gather within the grain interiors. The movement of some dislocations caused by the strengthening load will form a strip of parallel dislocations on one side of the grain boundaries if the grains are parallel in arrangement. That is to say, there is one dislocation strip having a higher density in each grain boundary. Dislocations in the grain interiors accumulate at grain boundaries if the grains are irregular. Both sides of each grain boundary have high-density dislocation straps.

In order to further investigate the distribution of dislocation lines within the grain interiors, the typical changes of dislocations in different specimens are shown in Fig. 5.

As shown in Fig. 5, there are some sparse and discrete dislocations in the virgin material because of an external force in the material molding process. In specimen No. 012 without SLAL, the dislocation density increased quickly within the grain interiors because of its initial overloading. The dislocation cells nearby the grain boundaries are easily broken down by new dislocations because the obstruction of dislocation movement is hardly established within the grain interiors. The dislocation density within the grain interiors always maintains a regular and relative saturation.

For the specimen No. 035, fractured by the same overload after being strengthened by the optimal strengthening load and cycle, new dislocations may be produced by the strengthening loads and clogged by the virgin dislocations. Dislocations accumulated within the grain interiors will cause the dislocation density to increase. These accumulated dislocations are called the dislocation wall. When the external force is small, a large amount of dislocation movement is blocked within the grain boundaries. Along with an increasing number of strengthening cycles, the dislocation density of the grain boundaries continuously increases to the saturation point and the high-density dislocation wall appears. These dislocations move within the grain interiors and must overcome and break the dislocation walls. Hence, the ability of grain anti-distortion is improved. The essence of strengthening under low-amplitude loads is that the grain boundaries are strengthened. This is the main reason why the fatigue strength and life are improved.

Figure 6 shows the TEM diffraction pattern for specimen No. 035 after SLAL. Apparently, the ferrite is a body-centered-cubic (bcc) lattice (Ref 24). The results of the axle length and interplanar spacing measured and computed through the diffraction patterns for different specimens are listed in Table 7. In Table 7, the axle length is distance between central spot and diffracted spot on left diffraction patterns in Fig. 6, and this is the diffraction for B = [001], then interplanar spacing "B axle" is interplanar distance for (200) planes and "C axle" interplanar distance for (110).

The interplanar spacing can be clearly changed if the specimen is subjected to high-amplitude loads. But the change in the interplanar spacing of specimen No. 035 is at first glance relatively smaller than that of the specimen without SLAL. The change in the interplanar spacing clearly increases if the specimen is directly subjected to a high overload. The larger the change in the interplanar spacing, the smaller the atomic bonding force in the unit cell.

3.4 XRD Experiments

The change in lattice constant for different specimens was measured by X-ray, and the result is shown in Table 8. The Lattice constant of ferrite is a = 0.28664 nm (Ref 24).

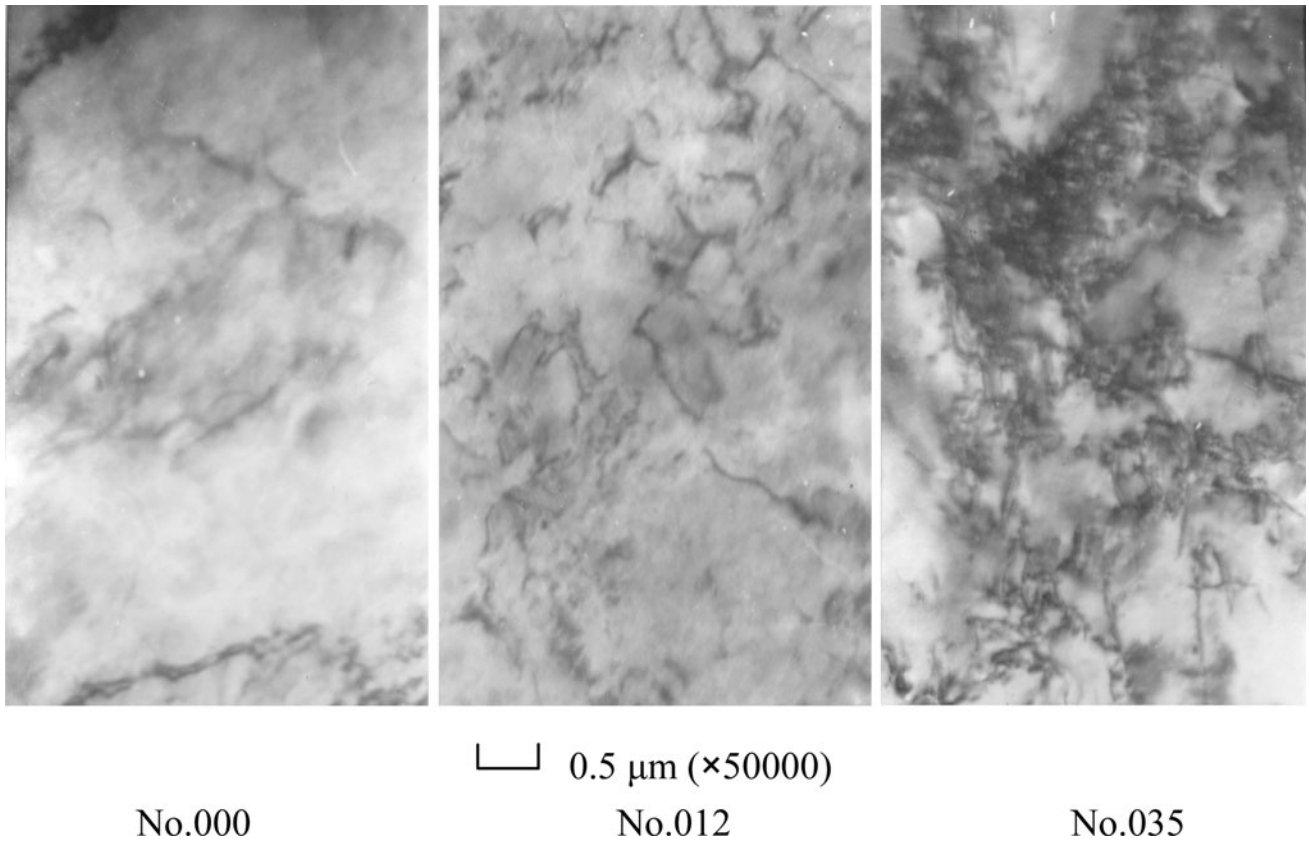

Fig. 5 Dislocation distribution of different specimens

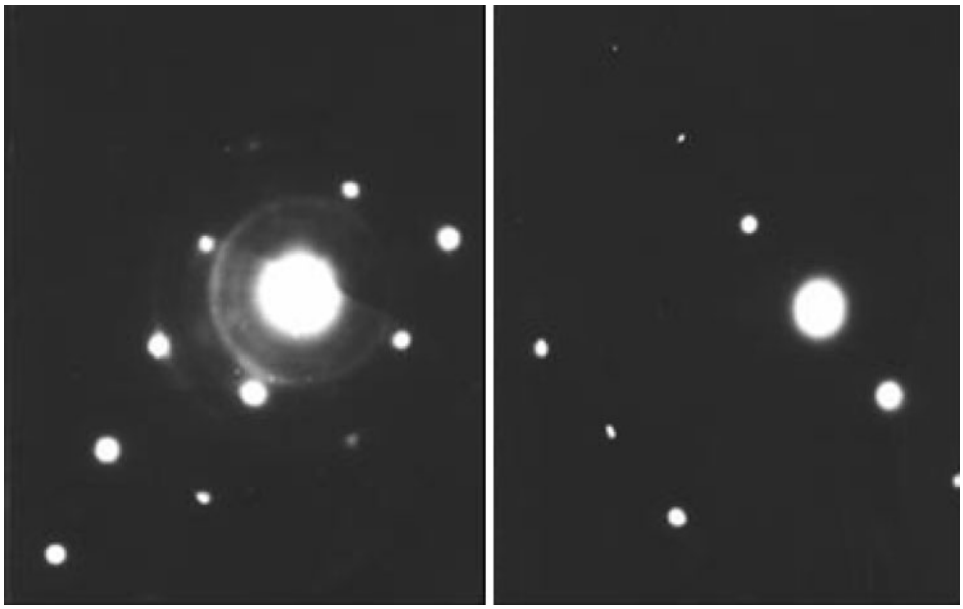

Fig. 6 Electron diffraction patterns in No. 035

Table 8 shows that the lattice constant of specimen No. 035 barely changes. However, the lattice constant of the specimen without SLAL increased by 10^{-4} nm. The damage in the crystal having a high load is restrained effectively by the SLAL. The reason for the improvement in the fatigue life and fatigue strength is that the ability of anti-distortion of crystals increased.

If the specimens are tested with high-amplitude loads directly, the crystal is not strengthened and the atomic bonding force of the unit cell is weak. The continuous increase in the

Table 7 Axle length and interplanar spacing in the different specimens

	Axle length, mm		Interplanar spacing, nm	
No.	B axle	C axle	B axle	C axle
000	15.25	10.75	0.14058	0.20269
012	15.00	10.67	0.14526	0.20421
035	15.33	10.80	0.14213	0.20176

Table 8 Lattice constant in the different specimens

	Lattice constant, nm			
No.	(110)	(200)	(211)	(220)
000	0.28672	0.28674	0.28664	0.28663
012	0.28672	0.28686	0.28674	…
035	0.28672	0.28674	0.28664	0.28663

atomic distance makes the lattice constant increase with repeated external forces. Therefore, the fatigue strength and fatigue life are decreased.

4. Discussion

The change of microstructure characteristics in a same specimen before and after SLAL can not be investigated in fatigue analysis. The differences will be unavoidably produced because different specimens are compared. However, there is a difference even though the same specimen is investigated because of the difference of measured positions. The number of specimens is too small to analyze statistically. Therefore, some figures are intercepted in an experimental image to emphasize the difference in different specimens. The incident direction of the electron beam and the calibration of spectrum diffraction are not discussed. So the conclusions are qualitative, relative, and primary, especially the amount of pores and secondary cracks, the dislocation distributions, the change of interplanar spacing and lattice constant require a statistical and quantitative analysis in the future.

Although the quantitative relationship between the strengthening effect and microstructure is not established, some comparative and quantitative results have been obtained, such as the crack propagation region, the diameter of pores, and the distance between beach marks. The results of experiments partially explain the micro-mechanism of the SLAL of a vehicle front axle.

5. Conclusions

The mechanism of the SLAL was investigated using microscopic experiments. Several conclusions were obtained as follows:

Comparing a virgin specimen to a specimen without strengthening, the specimen strengthened with the optimal parameters has smaller and fewer pores, fewer and thinner cracks, and a slower rate of crack propagating. These strengthened microstructures induce increased anti-fatigue characteristics.

After strengthening by the optimal strengthening effect, the dislocations within the gain interiors collect and form dislocation walls, which have large dislocation densities. Dislocation walls increase the friction between crystal lattices, inducing an anti-deformation effect. Thus, the fatigue life and strength of the structure are improved.

The lattice constant of the specimens without strengthening is significantly changed. However, it is almost constant for the specimen with the optimal strengthening effect. The reason may be that after strengthening with the optimal strengthening effect, the cohesive force among atoms within the crystal lattice as well as grain toughness is increased, and consequently the structural fatigue strength is increased.

Synthetically speaking, the mechanism of the SLAL is that under the cyclic action of inner stress caused by an appropriate low-amplitude load, dislocations within the grains are gradually moved to the grain boundaries. These dislocations accumulate along the grain boundaries, which act as obstacles to the movement of dislocations, thereby forming a dislocation wall. The strong strain energy gathered in the wall increases the friction among lattices and raises the local yield stress, so that the whole structure gets higher fatigue strength and longer fatigue life. In other words, the strengthened grain boundary is the key to the SLAL.

Acknowledgments

This work was supported by the National Natural Science Foundation of China (51175346, 50875173), Shanghai International Cooperation project (10520711500), and Innovation Program of Shanghai Municipal Education Commission (11YZ114).

References

1. H.J. Gough, *The Fatigue of Metals*, Scott, Greenwood and Son, London, 1924
2. G.M. Sinclair, An Investigation of the Coaxing Effect in Fatigue of Metals, *ASTM*, 1952, **52**(1952), p 743–758
3. Xi'an Jiaotong University, Special Issue for Materials of Metal and their Strength, Xi'an Jiaotong University Press, Xi'an 1972 (in Chinese)
4. W. Schlitz, A History of Fatigue, *Eng. Fract. Mech.*, 1996, **54**(2), p 263–300
5. T. Yamada, Fatigue Strength of Metallic Materials Under Varying Repeated Stresses, *Mater. Exp.*, 1957, **6**(45), p 373–377 (in Japanese)
6. T. Yamada and S. Kitagawa, Investigation of Fatigue Strength of Metals Under Actual Service Loads: With Two Superimposed Cyclic Loadings, *Bull. JSME*, 1967, **10**(38), p 245–252
7. H. Okubo and S. Kitaoka, Explanation of Understressing Affecting the Fatigue Strength, *J. Appl. Phys.*, 1968, **39**(5), p 2966–2968
8. J.J. Lawnicki and V.C. Cutler, Effect of Understressing and Coaxing on the Fatigue Limit of a Transverse Butt-Welded Joint, *J. Test. Eval.*, 1981, **9**(1), p 39–43
9. T. Nakagawa and Y. Ikai, Strain Ageing and the Fatigue Limit in Carbon Steel, *Fatigue Fract. Eng. Mater. Struct.*, 1979, **2**(1), p 13–21
10. L. Xi and Z. Songlin, Change of Mechanical Properties for Vehicle Components Strengthening Under Low-Amplitude Loads Below the Fatigue Limit, *Fatigue Fract. Eng. Mater. Struct.*, 2009, **32**(2), p 847–855
11. Z. Songlin, Studying the Effect of Low Amplitude Loading on Fatigue Life of Truck Front Axle, *J. Mech. Strength*, 2002, **24**(4), p 547–549 (in Chinese)

12. L. Xi and Z. Songlin, Strengthening of Transmission Gear Under Low-Amplitude Loads, *Mater. Sci. Eng. A-Struct.*, 2008, **488**(1–2), p 55–63
13. L. Jianhua and Z. Yajun, Influence of Training with Secondary Load on Bending Fatigue Strength of Crankshaft, *Modern Cast Iron*, 2001, **2**, p 23–24 (in Chinese)
14. H. Wenzheng, Z. Ping, Z. Jiliang et al., Investigation of In-Service Strengthening Characteristics of Tank Track Pans Made of Medium Manganese Cast Steel, *Ordnance Mater. Sci. Eng.*, 2000, **23**(4), p 3–6 (in Chinese)
15. L. Xi and Z. Songlin, Strengthening and Damaging Under Low-Amplitude Loads Below the Fatigue Limit, *Int. J. Fatigue*, 2009, **31**(2), p 341–345
16. M. Makajima, J. W. Jung, Y. Uematsu, and K. Tokaji, Coaxing Effect in Stainless Steels and High-Strength Steels, *Key Eng. Mater.*, 2007, **345–346**, p 235–238
17. S. Teimourimanesh and F. Nilsson, Effects of Cycles Below the Fatigue Limit on the Life of a High Strength Steel, *J. Test. Eval.*, 2009, **37**(3), p 201–204
18. C. Ngiau and D. Kujawski, Sequence Effects of Small Amplitude Cycles on Fatigue Initiation and Propagation in 2024–T351 Aluminum, *Int. J. Fatigue*, 2001, **23**(9), p 807–815
19. Y. Murakami, Y. Tazunoki, and T. Endo, Existence of the Coaxing Effect and Effects of Small Artificial Holes on Fatigue Strength of an Aluminum Alloy and 70–30 Brass, *Metall. Trans. A*, 1984, **15A**(11), p 2029–2038
20. A.B. El-Shabasy and J.J. Lewandowski, Fatigue Coaxing Experiments on a Zr-Based Bulk-Metallic Glass, *Scripta Mater.*, 2010, **62**(7), p 481–484
21. N. Kawagoishi, H. Nisitani, Y. Oda, and T. Toyohiro, Effect of Phase Morphology on Coaxing Effect of Dual-Phase Steels, *Trans. JSME-A*, 1994, **61**(528), p 339–345 (in Japanese)
22. Z. Qiong and C. Chuanrong, Deformation and Fracture of Pearlite in 35vb Steel After Loading Less than Fatigue Limit, *Mater. Mech. Eng.*, 1994, **18**(4), p 42–44 (in Chinese)
23. W. Zhixue, L. Wenge, and X. Hao, Study on Fatigue Damage Below the Fatigue Limit and the Coaxing Effects, *Acta Metall. Sin.*, 1996, **9**(3), p 227–231
24. H.P. Klug and L.E. Alexander, *X-Ray Diffraction Procedures: For Polycrystalline and Amorphous Materials*, Wiley-Interscience, New York, 1974